Analysis of Bifurcation Behaviors in MMC Connected to a Weak Grid

Haoxiang Zong, Jing Lyu, Xu Cai
Wind Power Research centre
Shanghai Jiaotong University
Shanghai, China
haoxiangzong@sjtu.edu.cn

Marta Molinas, Chen Zhang
Department of Engineering Cybernetics
Norwegian University of Science and Technology
Trondheim, Norwegian
marta.molinas@ntnu.no

Renxing Yang, Fangquan Rao
Wind Power Research centre
Shanghai Jiaotong University
Shanghai, China
frank_yang@sjtu.edu.cn

***Abstract*—Conventional small-signal approaches present obvious advantages applied in analyzing closed-loop stability in power electronics systems. However, linearized models fall short of predicting any nonlinear behavior which means not able to acquire the accurate stability margin. This paper mainly analyzes bifurcation behaviors of the Modular Multilevel Converter (MMC) connected to a weak grid and calculates the parameters' precise stability margin. The nonlinear continuous-time averaging model of the MMC is established to study two common bifurcation phenomena, i.e. Saddle-Node bifurcation (SNB) and Hopf bifurcation (HB). Characteristics of limit cycles caused by HB are analyzed by changing the value of a certain parameter. The theoretical analysis has been validated by the time domain simulation results.**

Keywords—MMC, bifurcation, limit cycles, stability margin

I. INTRODUCTION

The MMC has been widely used in high-voltage/high-power applications due to its advantages such as modularity, high efficiency, high performance, etc. However, it has complex internal structure which makes its modeling and control much more complicated. Due to this, affected by the MMC, stability problems of the power electronic system become more complex and difficult. Therefore, with consideration of the grid strength's effects, it's essential and meaningful to analyze the MMC's dynamic behavior which is closely associated with the system stability.

Currently, there are mainly two kinds of linear approaches to analyze MMC's small-signal stability, i.e. ,eigenvalue-based method [1] and impedance-based method [2], [3]. Nevertheless, both two methods neglect nonlinear characteristics and are only capable of characterizing the system behavior locally around a point in the state space, which means only the SNB [4] could be determined. The SNB is equivalent to the instability defined in small-signal approaches or Nyquist criterion, whereas dynamic bifurcations HB may bring about oscillatory instability which cannot be detected by linearized methods. More importantly, it's frequently observed in p wer system that HB and limit cycles lead to system collapse before the occurrence of the SNB [5]. Thus, the bifurcation theory is more suitable to study stability and oscillations of autonomous nonlinear systems, which is able to acquire the precise stability margin of the MMC's parameters with consideration of HB.

This work was supported by the National Key Research and Development Program under Grant 2016YFB0900901.

The bifurcation theory has been widely used to study voltage stability [5], oscillations [6] and stabilization [7] in power systems. In 1976, the bifurcation theory was first applied in analyzing sinusoidal electronic oscillator's periodic oscillations by Alistair [8]. Then the bifurcation and chaos behavior of dc-dc converters, e.g. cuk converter [9], buck converter [10], boost converter [11] etc. were analyzed. In recent years, bifurcation theory is expanded to power electronic systems. Based on multi-parameter bifurcation theory, [12] explains the mechanism of sub-synchronous oscillations between the wind farm and the grid. The voltage source converter's (VSC) catastrophic bifurcation phenomenon caused by voltage drop is analyzed in [13] by Huang et al. [14] analyzes the bifurcation of photovoltaic hybrid power system.

In this paper, the nonlinear continuous-time averaging model of a grid-connected MMC is established which considers circulating current and fluctuations of capacitor voltage. One-parameter bifurcation theory is adopted to reveal phenomena of SNB and HB. Also, characteristics of limit cycles derived from HB are studied. At last, time domain simulations are carried out to verify theoretical findings.

II. NONLINEAR CONTINUOUS-TIME AVERAGNING MODEL IN THE ABC FRAME

The nonlinear continuous-time averaging model derived in this paper consists of external dynamic model, internal dynamic model and control model. External dynamic model contains ac side's and dc side's dynamics. Internal dynamic model involves dynamic characteristics of capacitors' voltage and circulating current. The studied system is shown in Fig. 1, where the point of common coupling (PCC) is defined. The strength of power grid can be adjusted via short-circuit ratio (SCR). Control model is shown in Fig. 2 including the *d-q* decoupled control, phase locked loop (PLL) control and the circulating current suppress control (CCSC).

To make analytic analysis feasible, several assumptions need to be made before modeling: MMC works at three-phase balance status; capacitor's voltage balance of sub modules is ideal; PWM is represented by average model and sampling delay is neglected. The system parameters' definition and values are listed in TABLE I.

The MMC internal dynamics can be accurately represented

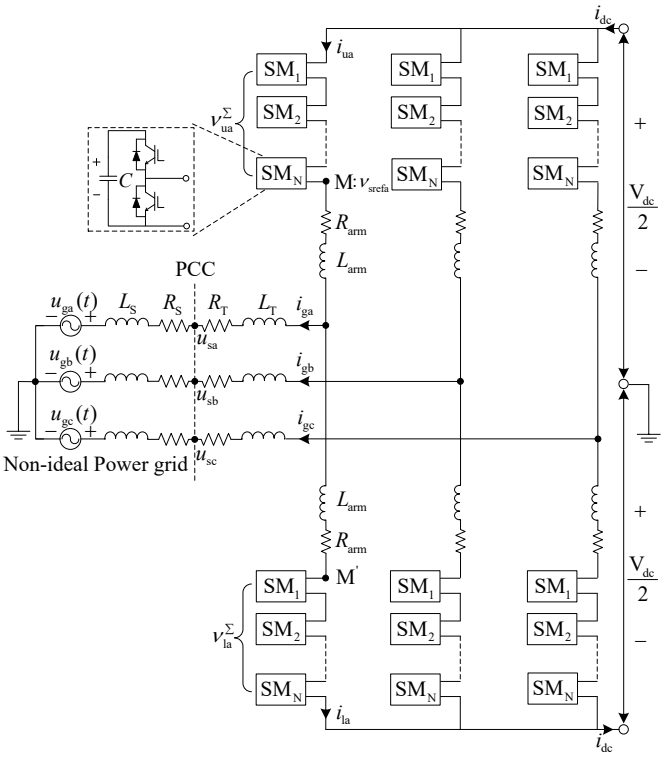

Fig. 1. The MMC connected to a weak grid

by the average model described in [15], which means only fundamental and second harmonic component exist. Components of each signal are listed in APPENDIX A. Thus, the converter dynamics in the three phases can be represented by the state- and control- variables defined in (1) and (2),

$$-2\omega:\ \boldsymbol{i}_{\mathrm{c}}=\frac{\boldsymbol{i}_{\mathrm{u}}+\boldsymbol{i}_{\mathrm{l}}}{2};\ \boldsymbol{v}_{\mathrm{c}}^{\Sigma}=\boldsymbol{v}_{\mathrm{cu}}^{\Sigma}+\boldsymbol{v}_{\mathrm{cl}}^{\Sigma} \tag{1}$$

$$+\omega:\ \boldsymbol{i}_{\mathrm{g}}=\boldsymbol{i}_{\mathrm{u}}-\boldsymbol{i}_{\mathrm{l}};\ \boldsymbol{v}_{\mathrm{c}}^{\Delta}=\boldsymbol{v}_{\mathrm{cu}}^{\Sigma}-\boldsymbol{v}_{\mathrm{cl}}^{\Sigma} \tag{2}$$

where $\boldsymbol{i}_{\mathrm{c}}$ and $\boldsymbol{i}_{\mathrm{g}}$ are the circulating and ac-side current state variables, while $\boldsymbol{v}_{\mathrm{c}}^{\Sigma}$ and $\boldsymbol{v}_{\mathrm{c}}^{\Delta}$ are the sum and difference of the aggregated upper and lower capacitor voltages (i.e. $\boldsymbol{v}_{u}^{\Sigma}$ and $\boldsymbol{v}_{\mathrm{l}}^{\Sigma}$). $\boldsymbol{i}_{\mathrm{u}}$ and $\boldsymbol{i}_{\mathrm{l}}$ are the upper and lower bridge arm current. Note that the chosen $\sum$-Δ representation allows for the separation of the state and control variables defined in (1)- (2) into two groups [16]: those mainly oscillating at -2ω ($\boldsymbol{i}_{\mathrm{c}}$, $\boldsymbol{v}_{\mathrm{c}}^{\Sigma}$) given in (1), and those oscillating at $+\omega$ ($\boldsymbol{i}_{\mathrm{g}}$, v_{c}^{Δ}) given in (2).

The upper and lower arm's modulation function $\boldsymbol{n}_{\mathrm{u}}$, $\boldsymbol{n}_{\mathrm{l}}$ can be acquired by normalizing voltage modulation wave. Direct modulation [16] is taken in this paper which means setting dc side voltage as reference value. The modulation function considering CCSC is given in (3) .

$$\begin{cases}\boldsymbol{n}_{\mathrm{u}}=\dfrac{\mathrm{V}_{\mathrm{dc}}/2-\boldsymbol{v}_{\mathrm{sref}}-\boldsymbol{v}_{\mathrm{cref}}}{\mathrm{V}_{\mathrm{dc}}}\\ \boldsymbol{n}_{\mathrm{l}}=\dfrac{\mathrm{V}_{\mathrm{dc}}/2+\boldsymbol{v}_{\mathrm{sref}}-\boldsymbol{v}_{\mathrm{cref}}}{\mathrm{V}_{\mathrm{dc}}}\end{cases} \tag{3}$$

where $\boldsymbol{v}_{\mathrm{sref}}$ is the output modulation voltage of dq coupled control, and $\boldsymbol{v}_{\mathrm{cref}}$ is the compensation output modulation voltage

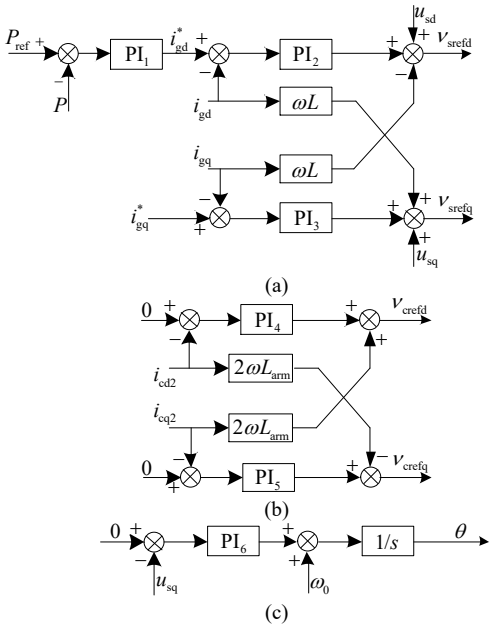

Fig. 2. Control block diagram of the MMC. (a) *d-q* decoupled control. (b) circulating current suppress control. (c) PLL transfer function.

of CCSC. According to [16], the state-space model of a three-phase MMC in a stationary reference frame is given in (4)-(8).

$$L\cdot\dot{\boldsymbol{i}}_{\mathrm{g}}+R\cdot\boldsymbol{i}_{\mathrm{g}}=\boldsymbol{v}_{\mathrm{sref}}-\boldsymbol{u}_{\mathrm{s}} \tag{4}$$

$$L_{\mathrm{s}}\cdot\dot{\boldsymbol{i}}_{\mathrm{g}}+R_{\mathrm{s}}\cdot\boldsymbol{i}_{\mathrm{g}}=\boldsymbol{u}_{\mathrm{s}}-\boldsymbol{u}_{\mathrm{g}} \tag{5}$$

$$L_{\mathrm{arm}}\cdot\dot{\boldsymbol{i}}_{\mathrm{c}}+R_{\mathrm{arm}}\cdot\boldsymbol{i}_{\mathrm{c}}=[\mathrm{V}_{\mathrm{dc}}-(\boldsymbol{n}_{\mathrm{u}}\cdot\boldsymbol{v}_{\mathrm{cu}}^{\Sigma}+\boldsymbol{n}_{\mathrm{l}}\cdot\boldsymbol{v}_{\mathrm{cl}}^{\Delta})]/2 \tag{6}$$

$$C\cdot\dot{\boldsymbol{v}}_{\mathrm{c}}^{\Sigma}=N\cdot(\boldsymbol{n}_{\mathrm{u}}\cdot\boldsymbol{i}_{\mathrm{u}}+\boldsymbol{n}_{\mathrm{l}}\cdot\boldsymbol{i}_{\mathrm{l}}) \tag{7}$$

$$C\cdot\dot{\boldsymbol{v}}_{\mathrm{c}}^{\Delta}=N\cdot(\boldsymbol{n}_{\mathrm{u}}\cdot\boldsymbol{i}_{\mathrm{u}}-\boldsymbol{n}_{\mathrm{l}}\cdot\boldsymbol{i}_{\mathrm{l}}) \tag{8}$$

With $\boldsymbol{n}_{\mathrm{u}}$ and $\boldsymbol{n}_{\mathrm{l}}$ in (3) substituted, equations (4)-(8) could be represented purely by state variables and control variables.

III. NONLINEAR CONTINUOUS-TIME AVERAGING MODEL IN THE DQ FRAME

To interface the control system, the electrical model derived above in the *abc* frame needs to be transformed to that in the *d-q* frame. The nonlinear multiplication terms in the *abc* frame for modulating oscillating signals exist in the equation derived in section II. According to [17], simultaneous modeling of these nonlinear terms in zero sequence, fundamental frequency DQ and double fundamental frequency DQ2 frames in the *d-q* frame are derived below.

A. Fundamental frequency dynamics

1) AC side: The voltage $\boldsymbol{u}_{\mathrm{s}}$ in the *d-q* frame at the PCC can be gotten in (9) by subtracting (4) from (5).

TABLE I. PARAMETERS DEFINITION

Parameters	Definition	Value
$\boldsymbol{u}_{\mathrm{g}}$	Ideal AC phase voltage	135.5 kV
$\mathrm{V_{dc}}$	DC voltage	±160 kV
L_{T}	Transformer equivalent inductance	0.035 H
R_{T}	Transformer equivalent resistance	1 Ω
L_{arm}	Arm inductance	0.06 H
R_{arm}	Arm resistance	2 Ω
L_{s}	Grid inductance	0.1 H
R_{s}	Grid resistance	1 Ω
C	Capacitance of sub modules	10 mF
N	Number of sub modules per arm	10
P_{ref}	Active power reference	500 MW

$$\begin{bmatrix} u_{sd} \\ u_{sq} \end{bmatrix} = \frac{1}{L_s + L}\begin{bmatrix} L\cdot R_s - L_s\cdot R & 0 \\ 0 & L\cdot R_s - L_s\cdot R \end{bmatrix}\cdot\begin{bmatrix} i_{\mathrm{gd}} \\ i_{\mathrm{gq}} \end{bmatrix} + \frac{1}{L_s + L}\begin{bmatrix} L\cdot u_{\mathrm{gd}} + L_s\cdot v_{\mathrm{srefd}} \\ L\cdot u_{\mathrm{gq}} + L_s\cdot v_{\mathrm{srefq}} \end{bmatrix} \tag{9}$$

The ac-side current of (4) is transformed into (10) in the DQ frame.

$$\frac{\mathrm{d}}{\mathrm{d}t}\begin{bmatrix} i_{\mathrm{gd}} \\ i_{\mathrm{gq}} \end{bmatrix} = \begin{bmatrix} -R/L & \omega \\ -\omega & -R/L \end{bmatrix}\cdot\begin{bmatrix} i_{\mathrm{gd}} \\ i_{\mathrm{gq}} \end{bmatrix} + \frac{1}{L}\cdot\begin{bmatrix} v_{\mathrm{srefd}} - u_{\mathrm{sd}} \\ v_{\mathrm{srefq}} - u_{\mathrm{sq}} \end{bmatrix} \tag{10}$$

where $\mathrm{L}=L_{\mathrm{T}}+L_{\mathrm{arm}}/2$, $\mathrm{R}=R_{\mathrm{T}}+R_{\mathrm{arm}}/2$.

2) Differential mode voltage: the differential mode voltage of (8) is transformed into (11) in the DQ frame.

$$\frac{\mathrm{d}}{\mathrm{d}t}\begin{bmatrix} v_{\mathrm{cd}}^{\Delta} \\ v_{\mathrm{cq}}^{\Delta} \end{bmatrix} = \begin{bmatrix} 0 & \omega \\ -\omega & 0 \end{bmatrix}\cdot\begin{bmatrix} v_{\mathrm{cd}}^{\Delta} \\ v_{\mathrm{cq}}^{\Delta} \end{bmatrix} + \begin{bmatrix} Z_{\mathrm{d}}^{\Delta} \\ Z_{\mathrm{q}}^{\Delta} \end{bmatrix} \tag{11}$$

where Z_{d}^{Δ} and Z_{q}^{Δ} are the nonlinear product of modulation signal.

$$\begin{aligned} Z_{\mathrm{d}}^{\Delta} = &-\frac{2N}{C\mathrm{V_{dc}}}(v_{\mathrm{srefd}}\cdot i_{\mathrm{co}} + \frac{1}{2}i_{\mathrm{cd2}}\cdot v_{\mathrm{srefd}} + \frac{1}{2}i_{\mathrm{cq2}}\cdot v_{\mathrm{srefq}}) \\ &+ \frac{N}{2C}i_{\mathrm{gd}} - \frac{N}{C\mathrm{V_{dc}}}(\frac{1}{2}i_{\mathrm{gd}}\cdot v_{\mathrm{crefd}} + \frac{1}{2}i_{\mathrm{gq}}\cdot v_{\mathrm{crefq}}) \end{aligned} \tag{12}$$

$$\begin{aligned} Z_{\mathrm{q}}^{\Delta} = &-\frac{2N}{C\mathrm{V_{dc}}}(v_{\mathrm{srefq}}\cdot i_{\mathrm{co}} - \frac{1}{2}i_{\mathrm{cd2}}\cdot v_{\mathrm{srefq}} + \frac{1}{2}i_{\mathrm{cq2}}\cdot v_{\mathrm{srefd}}) \\ &+ \frac{N}{2C}i_{\mathrm{gq}} - \frac{N}{C\mathrm{V_{dc}}}(-\frac{1}{2}i_{\mathrm{gq}}\cdot v_{\mathrm{crefd}} + \frac{1}{2}i_{\mathrm{gd}}\cdot v_{\mathrm{crefq}}) \end{aligned} \tag{13}$$

B. Zero sequence and second harmonic dynamics

1) DC side: circulating current of (6) is transformed into (14) in the DQ2 frame.

$$\frac{\mathrm{d}}{\mathrm{d}t}\begin{bmatrix} i_{\mathrm{co}} \\ i_{\mathrm{cd2}} \\ i_{\mathrm{cq2}} \end{bmatrix} = \begin{bmatrix} -\frac{R_{\mathrm{arm}}}{L_{\mathrm{arm}}} & 0 & 0 \\ 0 & -\frac{R_{\mathrm{arm}}}{L_{\mathrm{arm}}} & 2\omega \\ 0 & -2\omega & -\frac{R_{\mathrm{arm}}}{L_{\mathrm{arm}}} \end{bmatrix}\cdot\begin{bmatrix} i_{\mathrm{co}} \\ i_{\mathrm{cd2}} \\ i_{\mathrm{cq2}} \end{bmatrix} + \frac{1}{L_{\mathrm{arm}}}\cdot\begin{bmatrix} Z_{\mathrm{o}}^{\mathrm{c}} \\ Z_{\mathrm{d2}}^{\mathrm{c}} \\ Z_{\mathrm{q2}}^{\mathrm{c}} \end{bmatrix} \tag{14}$$

where $Z_{\mathrm{o}}^{\mathrm{c}}$, $Z_{\mathrm{d2}}^{\mathrm{c}}$ and $Z_{\mathrm{q2}}^{\mathrm{c}}$ are nonlinear products in the dq frame.

$$Z_{\mathrm{d2}}^{\mathrm{c}} = -\frac{1}{4}v_{\mathrm{cd2}}^{\Sigma} + \frac{1}{2\mathrm{V_{dc}}}v_{\mathrm{crefd}}\cdot v_{\mathrm{co}}^{\Sigma} + \frac{1}{4\mathrm{V_{dc}}}(v_{\mathrm{srefd}}\cdot v_{\mathrm{cd}}^{\Delta} - v_{\mathrm{srefq}}\cdot v_{\mathrm{cq}}^{\Delta}) \tag{15}$$

$$Z_{\mathrm{q2}}^{\mathrm{c}} = -\frac{1}{4}v_{\mathrm{cq2}}^{\Sigma} + \frac{1}{2\mathrm{V_{dc}}}v_{\mathrm{crefq}}\cdot v_{\mathrm{co}}^{\Sigma} + \frac{1}{4\mathrm{V_{dc}}}(v_{\mathrm{srefq}}\cdot v_{\mathrm{cd}}^{\Delta} + v_{\mathrm{srefd}}\cdot v_{\mathrm{cq}}^{\Delta}) \tag{16}$$

$$\begin{aligned} Z_{\mathrm{o}}^{\mathrm{c}} = &\frac{1}{4\mathrm{V_{dc}}}(v_{\mathrm{crefd}}\cdot v_{\mathrm{cd2}}^{\Sigma} + v_{\mathrm{crefq}}\cdot v_{\mathrm{cq2}}^{\Sigma} + v_{\mathrm{srefd}}\cdot v_{\mathrm{cd}}^{\Delta} + v_{\mathrm{srefq}}\cdot v_{\mathrm{cq}}^{\Delta}) \\ &+ \mathrm{V_{dc}}/2 - v_{\mathrm{co}}^{\Sigma}/4 \end{aligned} \tag{17}$$

2) Common mode voltage : the common mode voltage of (7) is transformed into (18) in the DQ2 frame.

$$\frac{\mathrm{d}}{\mathrm{d}t}\begin{bmatrix} v_{\mathrm{co}}^{\Sigma} \\ v_{\mathrm{cd2}}^{\Sigma} \\ v_{\mathrm{cq2}}^{\Sigma} \end{bmatrix} = \begin{bmatrix} 0 & 0 & 0 \\ 0 & 0 & 2\omega \\ 0 & -2\omega & 0 \end{bmatrix}\cdot\begin{bmatrix} v_{\mathrm{co}}^{\Sigma} \\ v_{\mathrm{cd2}}^{\Sigma} \\ v_{\mathrm{cq2}}^{\Sigma} \end{bmatrix} + \begin{bmatrix} Z_{\mathrm{o}}^{\Sigma} \\ Z_{\mathrm{d2}}^{\Sigma} \\ Z_{\mathrm{q2}}^{\Sigma} \end{bmatrix} \tag{18}$$

where Z_{o}^{Σ}, Z_{d2}^{Σ} and Z_{q2}^{Σ} are nonlinear products in the dq frame.

$$Z_{\mathrm{d2}}^{\Sigma} = \frac{N}{C}i_{\mathrm{cd2}} - \frac{2N}{C\mathrm{V_{dc}}}v_{\mathrm{crefd}}\cdot i_{\mathrm{co}} - \frac{N}{2C\mathrm{V_{dc}}}(v_{\mathrm{srefd}}\cdot i_{\mathrm{gd}} - v_{\mathrm{srefq}}\cdot i_{\mathrm{gq}}) \tag{19}$$

$$Z_{\mathrm{q2}}^{\Sigma} = \frac{N}{C}i_{\mathrm{cq2}} - \frac{2N}{C\mathrm{V_{dc}}}v_{\mathrm{crefq}}\cdot i_{\mathrm{co}} - \frac{1}{2C\mathrm{V_{dc}}}(v_{\mathrm{srefq}}\cdot i_{\mathrm{gd}} + v_{\mathrm{srefd}}\cdot i_{\mathrm{gq}}) \tag{20}$$

$$\begin{aligned} Z_{\mathrm{o}}^{\Sigma} = &-\frac{N}{C\mathrm{V_{dc}}}(v_{\mathrm{crefd}}\cdot i_{\mathrm{cd2}} + v_{\mathrm{crefq}}\cdot i_{\mathrm{cq2}} + \frac{v_{\mathrm{srefd}}\cdot i_{\mathrm{gd}} + v_{\mathrm{srefq}}\cdot i_{\mathrm{gq}}}{2}) \\ &+ \frac{N}{C}\cdot i_{\mathrm{co}} \end{aligned} \tag{21}$$

C. Control equations

The control equations in the DQ frame can be referred to [17] which are listed in (22).

$$\begin{cases} i_{\mathrm{gdref}} = (k_{\mathrm{p1}} + \dfrac{k_{\mathrm{i1}}}{s})\cdot\left[P_{\mathrm{ref}} - \dfrac{3}{2}(u_{\mathrm{sd}}\cdot i_{\mathrm{gd}} + u_{\mathrm{sq}}\cdot i_{\mathrm{gq}})\right] \\ v_{\mathrm{srefd}} = -i_{\mathrm{gq}}\cdot\omega L + (k_{\mathrm{p2}} + \dfrac{k_{\mathrm{i2}}}{s})\cdot(i_{\mathrm{gdref}} - i_{\mathrm{gd}}) + u_{\mathrm{sd}} \\ v_{\mathrm{srefq}} = i_{\mathrm{gd}}\cdot\omega L + (k_{\mathrm{p3}} + \dfrac{k_{\mathrm{i3}}}{s})\cdot(0 - i_{gq}) + u_{\mathrm{sq}} \\ v_{\mathrm{crefd}} = i_{\mathrm{cq2}}\cdot 2\omega L_{\mathrm{arm}} + (k_{\mathrm{p4}} + \dfrac{k_{\mathrm{i4}}}{s})\cdot(0 - i_{\mathrm{cd2}}) \\ v_{\mathrm{crefq}} = -i_{\mathrm{cd2}}\cdot 2\omega L_{\mathrm{arm}} + (k_{\mathrm{p5}} + \dfrac{k_{\mathrm{i5}}}{s})\cdot(0 - i_{\mathrm{cq2}}) \\ \omega = \omega_0 + (k_{\mathrm{p6}} + \dfrac{k_{\mathrm{i6}}}{s})\cdot(0 - u_{\mathrm{sq}}) \end{cases} \tag{22}$$

where k_{pi}(i=1~6) is PI_i's proportional adjustment factor, while k_{ii}(i=1~6) is PI_i's integral adjustment factor shown in Fig .2. By integrating formulae (9)-(22), the whole system's differential algebraic equations (DAE) is shown in (23)

$$\begin{cases} \dot{\boldsymbol{x}} = f(\boldsymbol{x}, \boldsymbol{y}, \boldsymbol{\mu}) \\ 0 = g(\boldsymbol{x}, \boldsymbol{y}, \boldsymbol{\mu}) \end{cases} \tag{23}$$

where $\boldsymbol{x}$, $\boldsymbol{y}$ and $\boldsymbol{\mu}$ represent state variables, algebraic variables, parameter variables respectively. Based on implicit function theorem, formulae (23) can be simplified to (24).

$$\dot{\boldsymbol{x}} = F(\boldsymbol{x}, \boldsymbol{\mu}) \tag{24}$$

Now the automatous multi-parameter nonlinear ordinary differential equations(ODE) of MMC is acquired .

IV. Stability Theory Based on Local Bifurcation

Bifurcation theory is mainly used to analyze qualitative changes of dynamic system caused by parameters' changes. To be specific, the theory keeps tracking the equilibrium solution without linearizing and studies characteristics of each balance point. However, Small-signal analysis neglects nonlinear terms existing in the ODE and is not able to analyze nonlinear behaviors.

A. Basic theory

A dynamical system can have multiple equilibrium solutions. For a given set of parameters and initial condition, the system converges to one of the equilibrium solutions. As the parameters vary, the presently assumed equilibrium solution becomes unstable and the system is attracted to another stable equilibrium solution. This phenomenon is termed bifurcation. In general, bifurcation can be regarded as a sudden change of qualitative behavior of a system when a parameter is varied. We may therefore classify bifurcation according to the type of qualitative change that takes place when a parameter μ is varied [4].

Two types of bifurcation are closely associated with the instability and/or collapse in power systems: SNB and HB. The SNB is characterized by a sudden loss or acquisition of a stable equilibrium solution as a parameter moves across a critical value. The HB is characterized by a sudden expansion of a stable fixed point to a stable limit cycle.

B. Detection of bifurcation points

There are mainly three ways to track the bifurcation point of a nonlinear system which are direct method, continuous method and optimal method respectively. The direct method is taken in this paper to calculate the SNB and HB for its high precision. Also the continuous method tracking balance manifold is used in section V via auto-07p [18] to verify the correctness of the direct method.

The basic principle of the direct method is to solve the nonlinear algebraic equation satisfied by local bifurcation. Newton method can be used because it converges fast. The remaining parameters of the system are fixed considering a single parameter system. Setting the eigenvalues and right eigenvectors of $D_xF(\boldsymbol{x},\mu)$ as λ and $\boldsymbol{u}_x$ respectively.

$$\boldsymbol{D}_x \boldsymbol{u}_x = \lambda \boldsymbol{u}_x \tag{25}$$

Let $\lambda(\mu)=\alpha(\mu)\pm i\beta(\mu)$, $\boldsymbol{u}_x = \boldsymbol{u}_{xR}+j\boldsymbol{u}_{xI}$

$$\begin{cases} \boldsymbol{D}_x \cdot \boldsymbol{u}_{xR} = \alpha \cdot \boldsymbol{u}_{xR} - \beta \cdot \boldsymbol{u}_{xI} \\ \boldsymbol{D}_x \cdot \boldsymbol{u}_{xI} = \alpha \cdot \boldsymbol{u}_{xI} + \beta \cdot \boldsymbol{u}_{xR} \end{cases} \tag{26}$$

Normalization equation of state-variables is $\boldsymbol{u}_x^{\mathrm{T}}\boldsymbol{u}_x=1$.

$$\begin{cases} \boldsymbol{u}_{xR}^{\mathrm{T}}\boldsymbol{u}_{xR} - \boldsymbol{u}_{xI}^{\mathrm{T}}\boldsymbol{u}_{xI} - 1 = 0 \\ \boldsymbol{u}_{xR}^{\mathrm{T}}\boldsymbol{u}_{xR} + \boldsymbol{u}_{xI}^{\mathrm{T}}\boldsymbol{u}_{xI} = 0 \end{cases} \tag{27}$$

The equilibrium point constraint equation is

$$0 = F(\boldsymbol{x}, \boldsymbol{\mu}) \tag{28}$$

By integrating formulae (26), (27), (28), the bifurcation point can be calculated according to the definition of HB ($\alpha=0\&\beta\neq0$) and SNB ($\lambda=0$, $\alpha=0\&\beta=0$).

C. Hopf bifurcation theory

The system maybe unstable for occurrence of HB before generating saddle-point. Considering a single parameter system.

$$\dot{\boldsymbol{x}} = f(\boldsymbol{x}, \mu) \tag{29}$$

When bifurcation occurs at $(\boldsymbol{x}_0,\mu_0)$, the translation transformation from original equilibrium point $(\boldsymbol{x}_0,\mu_0)$ to $(\boldsymbol{0},0)$ is implemented. According to center manifold theory [4], the system has a two-dimensional central manifold at the equilibrium point($\mu=\mu_0$) which can transform n-dimensional bifurcation into two-dimensional bifurcation. The simplified two-dimensional system is represented as

$$\dot{\boldsymbol{x}} = f(\boldsymbol{x}, \mu)\ , \boldsymbol{x} \in \mathbf{R}^2,\ \mu \in \mathbf{R} \tag{30}$$

Taylor expansion is implemented as

$$\dot{\boldsymbol{x}} = \boldsymbol{A}(\mu)\boldsymbol{x} + f_2(\boldsymbol{x}) + f_3(\boldsymbol{x})\ , \boldsymbol{x} \in \mathbf{R}^2,\ \mu \in \mathbf{R} \tag{31}$$

Theorem: When (0,0) is non-hyperbola equilibrium point and $\boldsymbol{D}_xF(\boldsymbol{x}_0,\boldsymbol{\mu}_0)$ has a pair of pure virtual eigenvalues $\alpha(\mu)\pm i\beta(\mu)$ around $\mu=0$, there exists a analytic function in (31) with $\varepsilon_0>0$.

$$\mu(\varepsilon) = \sum_{i=2}^{\infty} \mu_i \cdot \varepsilon^i \tag{32}$$

When $\mu=\mu(\varepsilon)\neq0(\varepsilon \in (0, \varepsilon_0))$, the system has only one closed track(i.e. periodic solution Γ_ε) within a sufficiently small neighborhood of the origin. The analytic function of this periodic solution is represented as

$$x(s,\varepsilon) = \sum_{i=1}^{\infty} x_i(\varepsilon) \cdot \varepsilon^i \tag{33}$$

where $s=2\pi t/T$. The cycle of periodic solution is represented as

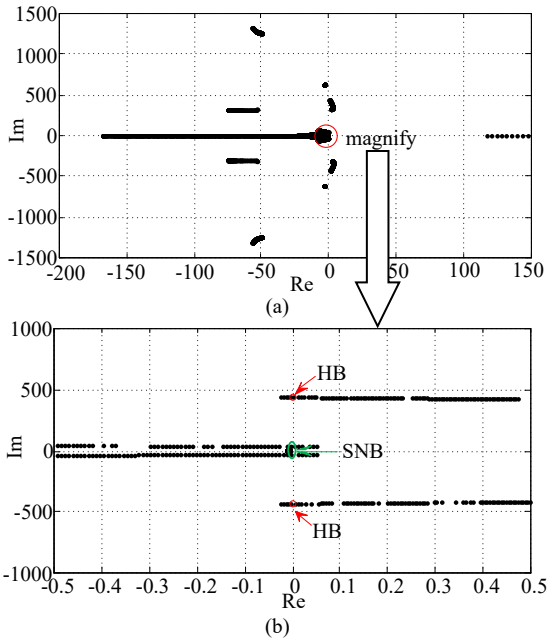

Fig. 3. Distribution of engivalues. (a) global distribution from k_{p2}=5 to k_{p2}=0; (b) partial enlarged detail around virtual axis.

$$T(\varepsilon)=\frac{2\pi}{\beta_0}(1+\sum_{i=2}^{\infty}\tau_i\varepsilon^i) \tag{34}$$

where coefficient μ_i can be calculated referring to [4].

With $\mu(\varepsilon)\to 0$ when $\varepsilon\to 0$, Γ_ε tends to the origin. Set μ_{j1} as the first non-zero coefficient of (32). If the sign of μ_{j1} and d is same, Γ_ε is a stable limit cycle defined as supercritical HB. And equal amplitude oscillations occur around the equilibrium point; If the sign of μ_{j1} and d is different, Γ_ε is an unstable limit cycle defined as subcritical HB. And the increasing amplitude oscillations occur around the equilibrium point.

V. Case Study

In this section, the proportional gain k_{p2} of inner current control loop is varied and the bandwidth remains unchanged. The bifurcation point is calculated via the algorithm proposed in Section I and the accuracy is verified by continuous method in auto-07p. Next, limit cycles are depicted to distinguish the bifurcation type which is validated by time domain simulations in Matlab. The accurate stable margin of proportional gain of the inner loop is acquired which can be extended to other parameters to get the global stable margin of MMC.

A. Calculation of bifurcation points

By using direct method, the algorithm converges after six iterations which consume 0.078s. The HB occurs at k_{p2}=0.46 and then SNB appears at k_{p2}=0.22. Contrast with the direct method, HB occurs at k_{p2}=0.467543 and then SNB appears at k_{p2}=0.228456 via continuous method. The movement of eigenvalues is shown in Fig. 3(a). From the Fig. 3(b), the oscillating frequency can be approximated which is about 70HZ.

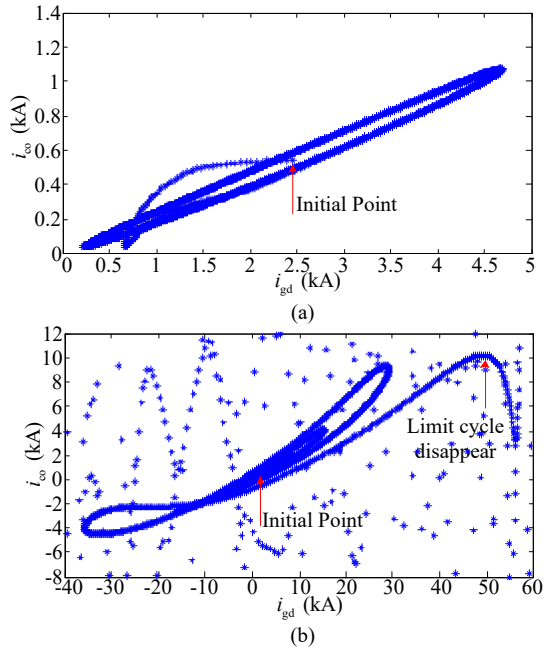

Fig. 4. Limit sycles. (a)stable limit cyles at HB(k_{p2}=0.46); (b)disappearance of limit cycles at SNB(k_{p2}=0.22).

B. Limit cyles

The state variable i_{co} and i_{gd} is chosen as horizontal and vertical axis variables of limit cycle because i_{co} is associated with output power of DC side while i_{gd} is associated with input power of AC side. When k_{p2} drops to 0.46, the structural stability of the system is damaged due to the HB. It can be seen from Fig. 4(a) that a stable limit cycle generates from HB not affected by small disturbances. It can be judged that this bifurcation belongs to the supercritical HB. However, the limit cycle disappears gradually when k_{p2} drops below 0.22 and the HB degenerates to the SNB.

C. Simulation validation in time domain

The i_{gd} is associated with the active power input P_{ac} of the system so its dynamics can be represented by P_{ac}. If k_{p2} drops from 5.0 to 0.46 at 0.02s, equal amplitude oscillations of P_{ac} are observed as shown in Fig. 5(a) which correspond to the stable limit cycle in Fig. 4(a). The oscillation frequency is about 65HZ which fits well with the HB's eigenvalue derived in part A. If k_{p2} drops from 0.46 to 0.22 at 0.02s, increasing amplitude oscillations of P_{ac} are observed as shown in Fig. 5(b) which correspond to the SNB in Fig. 4(b). Before the SNB, the system collapses at the HB for P_{ac}'s big oscillation amplitude.

VI. Conclusions

In this paper, bifurcation behaviors and limit cycles of the MMC connected to a weak grid are analyzed and theoretical results are verified by time domain simulations. The system's nonlinear continuous-time averaging model is first established considering circulating current and fluctuations of capacitors' voltage. By setting proportional gain of inner current loop as the free parameter, the HB and SNB point of the system is calculated. Limit cycles generated from the HB are analyzed

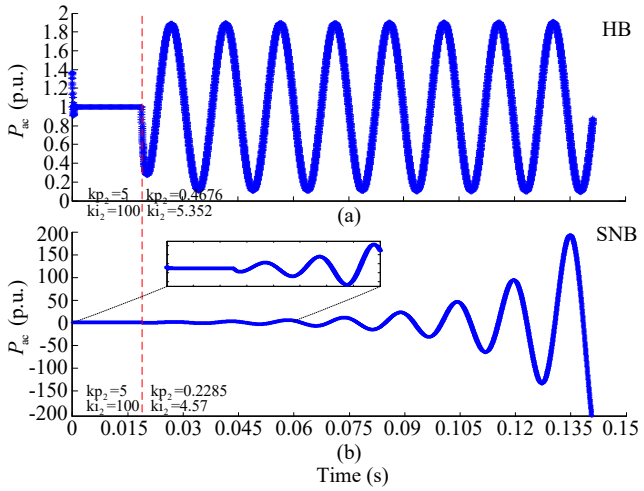

Fig. 5. Simulation verifications in time domain.

and compared with results of time domain simulations in Matlab. It's observed that the supercritical HB and limit cycles have caused the system collapse before the occurrence of the SNB. This phenomena explains the necessity to study nonlinear behaviors of the MMC since conventional small-signal analysis could only calculate the SNB which is not able to acquire the accurate stable margin.

Therefore, the method proposed in this paper is more rigorous than the small-signal method which is extremely meaningful for large disturbance analysis and accurate stability margin calculations. In the near future, the quantitative calculation of limit cycles will be done, which is able to reveal the instability mechanism of the MMC connected to the weak grids. Furthermore, the bifurcation control scheme will be designed to improve system's transient stability.

ACKNOWLEDGMENT

The authors would like to thank team members at SJTU, and co-workers from NTNU for their valuable advices.

APPENDIX A

Components of main signals are represented as follows:

$$i_g(t) = i_{gd} + i_{gq}$$
$$i_c(t) = i_{co} + i_{cd2} + i_{cq2}$$
$$v_c^{\Sigma} = v_{co}^{\Sigma} + v_{cd2}^{\Sigma} + v_{cq2}^{\Sigma}$$
$$v_c^{\Delta} = v_{cd}^{\Delta} + v_{cq}^{\Delta}$$
$$v_{cref} = v_{crefd} \cdot \cos(2\omega t) + v_{crefq} \cdot \sin(2\omega t)$$
$$v_{sref} = v_{srefd} \cdot \cos(\omega t) + v_{srefq} \cdot \sin(\omega t)$$

REFERENCES

[1] Saeedifard, Maryam, and R. Iravani, "Dynamic Performance of a Modular Multilevel Back-to-Back HVDC System," IEEE Transactions on Power Delivery, vol. 25, no. 4, pp. 2903-2912, Oct. 2010.

[2] J. Lyu, X. Zhang, X. Cai, and M. Molinas, "Harmonic state-space based small-signal impedance modeling of modular multilevel converter with consideration of internal harmonic dynamics," IEEE Transactions on Power Electronics, 2018, early access.

[3] J. Lyu, X. Cai, and M. Molinas, "Optimal design of controller parameters for improving the stability of MMC-HVDC for wind farm integration," IEEE Journal of Emerging and Selected Topics in Power Electronics, vol. 6, no. 1, pp. 40-53, Mar. 2018.

[4] Hassard, Brian D, N. D. Kazarinoff, and Y. H. Wan, Theory and applications of hopf bifurcation, Cambridge University Press, 1981.

[5] Abed, E. H, et al, "Dynamic bifurcations in a power system model exhibiting voltage collapse," 1992 IEEE International Symposium on Circuits and Systems, San Diego, CA, USA, 1992, pp. 2509-2512 vol.5.

[6] Abed, E. H., and P. P. Varaiya, "Nonlinear oscillations in power systems," International Journal of Electrical Power & Energy Systems, vol. 6, no. 1, pp. 37-43, 1984.

[7] Lerm, A., and A. Silva, "Avoiding hopf bifurcations in power systems via set-points tuning," IEEE Power Engineering Society General Meeting, 2004., Denver, CO, 2004, pp. 1714 Vol.2-.

[8] Mees, A, and L. O. Chua, "The Hopf bifurcation theorem and its applications to nonlinear oscillations in circuits and systems," IEEE Transactions on Circuits and Systems, vol. 26, no. 4, pp. 235-254, April 1979.

[9] Tse, C. K., Y. M. Lai, and H. H. C. Iu, "Hopf bifurcation and chaos in a free-running current-controlled Cuk switching regulator," IEEE Transactions on Circuits and Systems I: Fundamental Theory and Applications, vol. 47, no. 4, pp. 448-457, April 2000.

[10] Iu H. H. C, et al, "Bifurcation behaviour in parallel-connected Buck converters," IEEE Transactions on Circuits and Systems I: Fundamental Theory and Applications, vol. 48, no. 2, pp. 233-240, Feb. 2001.

[11] Parui, S, and S. Banerjee, "Bifurcations due to transition from continuous conduction mode to discontinuous conduction mode in the boost converter," IEEE Transactions on Circuits and Systems I: Fundamental Theory and Applications, vol. 50, no. 11, pp. 1464-1469, Nov. 2003.

[12] Revel, Gustavo, et al, "Multi-parameter bifurcation analysis of subsynchronous interactions in DFIG-based wind farms," Electric Power Systems Research, vol. 140, pp. 643-652, 2016.

[13] Huang, Meng, et al, "Catastrophic Bifurcation in Three-Phase Voltage-Source Converters," IEEE Transactions on Circuits and Systems I: Regular Papers, vol. 60, no. 4, pp. 1062-1071, April 2013.

[14] Huang, Meng, et al, "Bifurcation Based Stability Analysis of Photovoltaic-Battery Hybrid Power System," IEEE Journal of Emerging and Selected Topics in Power Electronics, vol. 5, no. 3, pp. 1055-1067, Sept. 2017.

[15] Antonopoulos, Antonios, L. Angquist, and H. P. Nee, "On dynamics and voltage control of the Modular Multilevel Converter," 2009 13th European Conference on Power Electronics and Applications, Barcelona, 2009, pp. 1-10.

[16] Bergna, Gilbert, J. A. Suul, and S. D'Arco, "State-space modelling of modular multilevel converters for constant variables in steady-state," 2016 IEEE 17th Workshop on Control and Modeling for Power Electronics (COMPEL), Trondheim, 2016, pp. 1-9.

[17] Jamshidifar, Aliakbar, and D. Jovcic, "Small-Signal Dynamic DQ Model of Modular Multilevel Converter for System Studies," 2016 IEEE Power and Energy Society General Meeting (PESGM), Boston, MA, 2016, pp. 1-1.

[18] Doedel, E. J., and B. E. Oldeman, "Auto-07P: Continuation and bifurcation software for ordinary differential equations, " vol. 10, no. 3, pp.531-535,2013.

View publication stats